Secondary and Backscatter Electron Emission Measurement

W. G. Wilson

AIR FORCE RESEARCH LABORATORY
Space Vehicles Directorate / Surveillance and Control Division
Space Electronics and Protection Branch (AFRL-VSSE)
Kirtland Air Force Base, NM 87117

Introduction:

This paper reports measurements of the secondary and backscatter electron energy and angle emission distributions from metals, generated by incident electrons with energies from ~100 eV to ~20 keV. When an energetic electron is incident on a solid surface, a considerable number of additional electrons may be produced; these electrons are called "secondary electrons" if emitted at energies below 50eV and "backscatter electrons" if emitted above 50 eV. The energy and angle integrated yield for most metals is less than one, but may be as large as 8 or more for insulators. There is a long history of secondary electron and backscatter electron measurements, mostly from metals at low incident energies. Relatively few measurements of the energy and angle distributions of the emitted electrons have been made. Even more limited is the data available for insulators and semiconductors used in spacecraft design. Spacecraft surface charging, differential charging and deep charging are controlled or augmented by secondary and backscatter electron emission. Secondary electron emission is an important feature of plasma-solid surface interactions, and may have considerable effects on the behavior of components such as solar cells in low earth orbit.

The yield data are presented as:

1) differential electron yield for secondary and backscatter electrons in units of $\#_{out}/\#_{in}$/sr/eV:

$$\frac{d^2\sigma}{dE d\Omega} = Y(E_p, \theta_p, M, E_s, \theta_s, \phi_s)$$

where E_p is the incident electron energy ($100\ eV \le E_p \le 20$ keV), θ_p is the off normal incident angle ($0^o \le \theta_p \le 80^o$) and M is the target set examined (here 1"x1" coupons of carbon, copper, brass, stainless steel and aluminum conductors). E_s ($0.02\ eV \le E_s \le E_p$) is the energy of the emitted electron while θ_s ($0^o \le \theta_s \le 80^o$) and ϕ_s ($0^o \le \phi_s \le 80^o$) are the in-and-out-of-plane emission angles. In the above, the 80^o values should ideally be 90^o, but were limited by vacuum mechanical constraints. The low energy cutoff at 0.02eV is discussed below.

2) secondary electron emission coefficient (δ) in units of $\#_{out}/\#_{in}$:

$$\delta(E_p, \theta_p, M) = \int \frac{d^2\sigma}{dE d\Omega} dE\, d\Omega$$

where the integral is over electron emission angles: θ_s, ϕ_s and over electron emission energy: $0 < E_s < 50$ eV.

3) backscatter electron emission coefficient (η), in units of $\#_{out}/\#_{in}$:

$$\eta(E_p, \theta_p, M) = \int \frac{d^2\sigma}{dE d\Omega} dE\, d\Omega$$

where the integral is over electron emission angles: θ_s, ϕ_s and over electron emission energy: $50\ eV < E_s < E_p$.

4) the total electron emission coefficient (σ) in units of $\#_{out}/\#_{in}$:

$$\sigma(E_p, \theta_p, M) = \delta + \eta.$$

The present measurements will feed a data base of electron emission coefficients (δ, η and σ) and energy and angle distributions of the emitted electrons (Y).

Technique:

The energy of the emitted electron is measured by timing the flight of the electron along a known path length (Time Of Flight: TOF). The secondary and backscatter electrons are created at time "zero" when an electron packet (at the selected incident energy E_p) hits the target material. The flight time of the emitted electron is then measured from the target to the detector. The main advantage of this technique is its simplicity - one need only measure length and time to determine the absolute electron energy. Problems with material contact potentials and work function differences are minimized, i.e., a reference energy calibration of the system is not required. As there is no electron optics on the emitted electron detection arm, no energy dependent transmission function need be determine. This technique can also be used to analyze the energy and charge state of excited or ionized species emitted from the

surface by particle bombardment (our laboratory is also interested in electron stimulated desorption). Use of a pulsed electron source minimizes incident beam/target interactions. There is minimal target surface modification due to sputtering of surface material, nor is there beam induced heating of the target (a typical power flux delivered to target is 3mW/cm^2). Likewise, there is minimal surface and deep charging effects on insulating target surfaces as the typical incident electron beam current is a DC equivalent of ~2pA (i.e., the incident electron pulse packet contains ~125 electrons). Because of the low currents involved, there is also minimal energy shifts due to space charge effects.

There are some compromises that must be made when using TOF: the low energy cutoff of the secondary emission spectrum is determined by either the residue magnetic field along the flight path or the flux of high energy electrons that arrive at the detector after scattering from chamber walls. Both of these effects are minimized if a short flight path (L) from the target to the detector is used. If good energy resolution at high emission energies is required a long flight path is needed. Since

$$\left(\frac{\Delta E}{E}\right)^2 = \left(2 * \frac{\Delta T}{T}\right)^2 + \left(2 * \frac{\Delta L}{L}\right)^2$$

very good energy resolution 'ΔE' is possible at low emission energies where the flight time (T) is long. Poorer resolution is obtained at high emission energies where the flight time is short. Therefore a compromise between low energy cutoff and energy resolution at high emission energies is necessary.

To maintain good energy resolution at higher energies, the incident electron beam must be delivered to the target in a packet with as small a time width as possible. A direct measure of the entire system time resolution 'ΔT' is obtained from the width of the X-ray flash generated when the incident electrons hit the target. This is a measure of both the temporal width of the electron packet and the time jitter of the processing electronics (a typical value for the timing resolution is 0.6 nsec FWHM). Using a more conservative 1 ns FWHM timing uncertainty results in an energy resolution of 8% at 20 keV emission energy.

In the low energy emission region, the energy resolution is limited by the physical size of the incident electron beam footprint on the target 'ΔL', i.e., the launch points of the emission electrons are spread out over a region parallel to the flight path. A worst case example would be that of a 1 mm diameter incident primary electron beam with an incident and detection angle of 80°. This will result in a flight path uncertainty, 'ΔL', of ~ 5 mm with a corresponding energy resolution of 1% at 1 eV emission energy. At near normal incident and detection angles, ΔL ~ .05 mm with a corresponding energy resolution of 0.01%.

There are three corrections that need to be made to any measured electron emission spectrum. The first is the removal of late arriving high energy electrons. At long flight times, the low energy spectra is contaminated with high energy electrons that reach the detector after multiple scatters from the chamber walls. These events are classified as low energy electrons based solely on the flight time. A separate measurement with the target displaced out of the direct field of view of the detector is used to correct the measured spectra for these late arrival high energy electrons (the offset spectrum contamination). Figure 1 is a typical electron emission spectrum, with overlays showing the measured offset spectrum normalized for the same charge delivered to the target and the final corrected emission spectrum off set by a multiplicative factor of 10 for display purposes.

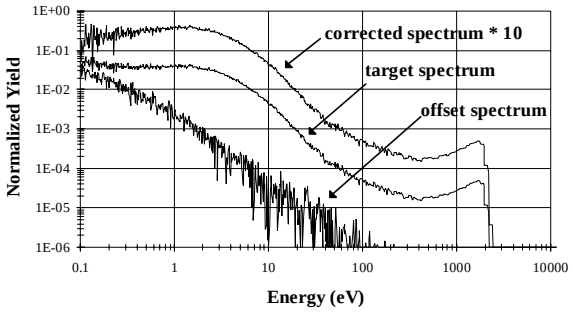

Figure 1 Carbon spectrum

A second correction is for the data acquisition system dead time. During a typical data run, the detector count rate could be ~2,000 cps at an electron packet pulse frequency of 10,000 Hz (these values are dependent on the value for the integrated electron yield σ, which is dependent on the incident electron energy and the target material). With this detector count rate, only one emission electron will be detected for every five electron packets hitting the target. Even at this low count rate, the data acquisition system is dead for ~ 15% of the time (because it is busy processing a previous TOF event) and is unable to accept a following event. The measured spectrum is therefore a spectrum of 'first arrivals' and not a spectrum of 'all arrivals.' The system dead time is monitored during all data runs and the measured emission spectrum is corrected for all of these missed events. Figure 2 is a record of the typical deadtime of the data acquisition system during a data run on copper.

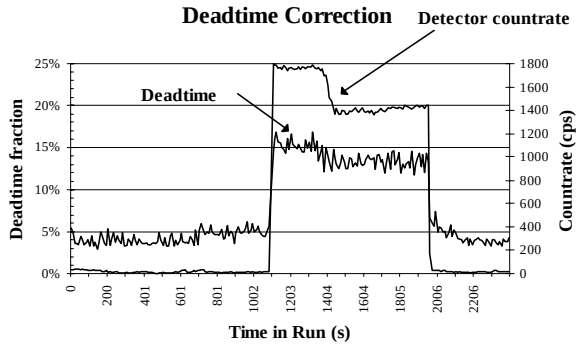

Figure 2:Acquisition System Deadtime

The last correction made to the emission spectrum is that for the detector efficiency. The efficiency of the microchannel plate (MCP) detector used to detect the emission electron is dependent on the incident electron energy. The absolute detection efficiency and the variation of this efficiency as a function of incident electron energy is measured independently and used to correct the measured electron emission spectrum. Figure 3 is the absolute efficiency of the MCP as a function of incident electron energy with the input surface of the MCP biased by +270V so as to improve the detection efficiency at low incident electron energy. The contribution to the detection efficiency do to secondary electron productin at the grid in front of the MCP is also shown.

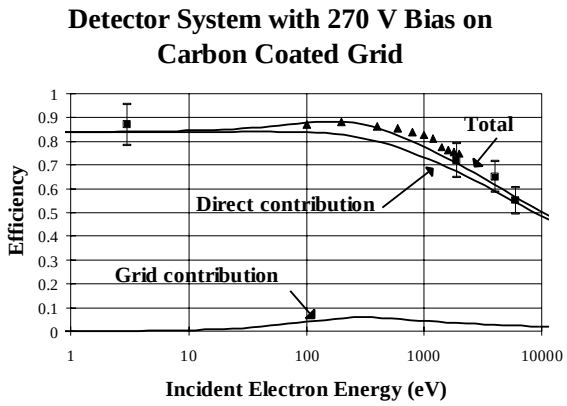

Figure 3 Absolute Detector Efficiency

Results:

Figure 4 is a typical secondary and backscattered emission spectrum for carbon. Most of the electron emission is at energies below 50 eV. Included on the plot are the integrated yields for secondary electrons ($\delta = 0.67$ for $E_s < 50$eV) and backscatter electrons ($\eta = 0.16$ for $E_s >$ 50eV). Figure 5 is the emission spectrum for aluminum at various incident energies.

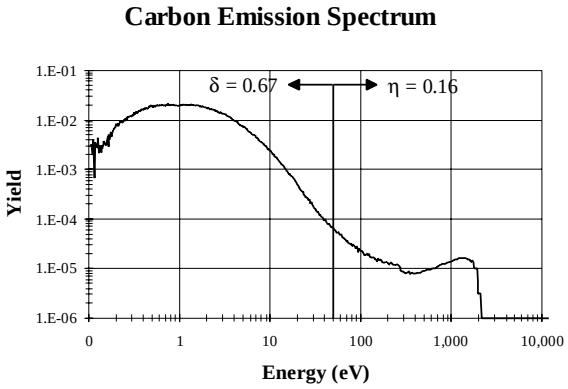

Figure 4: Carbon Spectrum

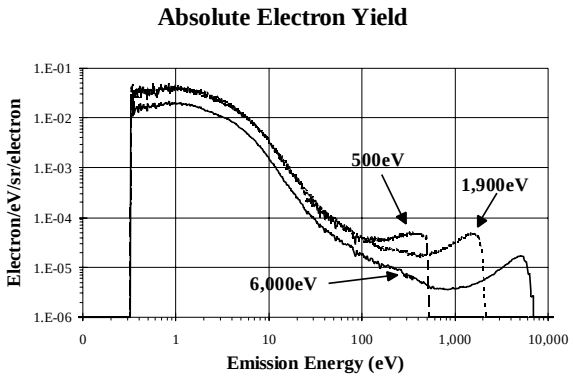

Figure 5: Aluminum emission spectrum.

The integrated data can be compared with various empirical expressions. The first comparison is with expressions currently used in the computer program from Katz (the codes NASCAP: NASA Charging Analyzer Program and DynaPAC: Dynamic Plasma Analysis Code, calculate spacecraft charging of satellites)[1]:

$$\delta_K = 1.114 * \frac{\delta_{max}}{\cos(\theta_p)} * R^{0.35} * \left(1 - e^{-2.28 * \cos(\theta_p) * R^{1.35}}\right)$$

and

$$\eta_K = S * \left(1 - \left(\frac{2}{E_p} \right)^{0.037 * Z} + 0.1 * e^{-\left(\frac{E_p}{5000} \right)} \right)$$

where $S = \ln(\frac{E_p}{50}) / \ln(20)$ for 50eV < E_p < 1000eV or S = 1 for E_p > 1000eV where E_p and θ_p are defined as above. R $= E_{max}/E_p$ where E_{max}, is the incident electron energy at the maximum secondary electron production coefficient (δ_{max}) and Z is the atomic number of the target material. A second comparison of the integrated data will be with the empirical expressions of Sternglass[2] and Prokopenko[3] (here only δ):

$$\delta_{SP} = 7.4 * \frac{\delta_{max}}{\cos(\theta_p)} * R * e^{-2*\sqrt{R}}.$$

Table 1 summarizes the measured values of δ, η and σ for carbon, copper and aluminum at various incident

Incident Energy (eV)	δ	+	η	=	σ
Aluminum:					
500	1.25 (1.23)	[1.28] +	0.15 (0.17)	=	1.40 (1.40)
1,900	0.79 (0.87)	[0.42] +	0.27 (0.33)	=	1.06 (1.13)
6,000	0.38 (0.74)	[0.28] +	0.28 (0.33)	=	0.66 (1.07)
Carbon:					
1,900	0.67 (0.83)	[0.44] +	0.16 (0.21)	=	0.84 (1.04)
Copper:					
1,900	1.29 (1.37)	[1.23] +	0.42 (0.33)	=	1.71 (1.70)

Table 1: Secondary (δ), backscatter (η) and total (σ) electron yield coefficients

energies. Included in this table are values for δ and η calculated using the Katz and Sternglass and Prokopenko expressions. Numbers not inclosed are the present measurements obtained by integrating the measured spectrum over angle and energy. Those in parenthesis are calculated using the Katz expression for δ (E_s < 50eV) and for η (E_s > 50eV), while those in brackets are calculated using the Sternglass/Prokopenko expression for δ (E_s < 50eV).

Another comparison of the present measurements is of the measured emission energy distributions with two expressions for the energy distribution of the emitted electrons. A Maxwellian distribution is given by:

$$\frac{dY}{dE} = A * (E_s)^n * e^{-\frac{E_s}{E_o}}$$

where "n" the Maxwellian exponent, E_s the energy of the emitted electron and E_0 an effective temperature related to the width of the distribution. The peak of the emission distribution is located at an emission energy given by

$$E_{peak} = n * E_o.$$

This expression is a valid representation for the energy dependence of the electron emission distribution from a heated metal (e.g., a tungsten filament at a temperature of T_0 = 1000K => E_0 = 0.08 eV and n=½) -- but a poor for the secondary electron emission energy distribution.

The second expression is from Hachenberg[4]:

$$\frac{dY}{dE} = A * \frac{E_s}{(E_s + \phi)^4}$$

here ϕ is the work function of the target material. This distribution peaks at

$$E_{peak} = \frac{\phi}{3}.$$

Figure 6 is a plot of the measured copper data compared with the calculated emission spectrum of Maxwell and Hachenberg. The Maxwellian expression has two parameters ("E_0" and "n") that can be adjusted to optimize

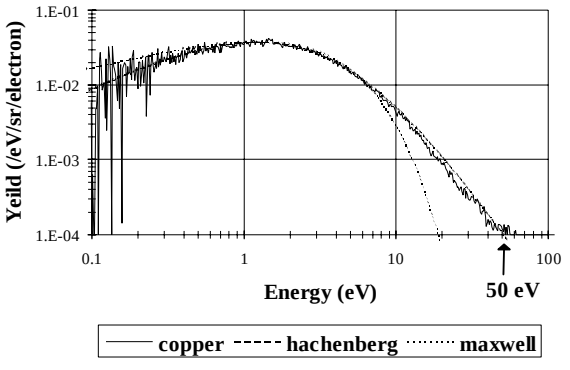

Figure 6: Low Energy Region for Copper

the fit to the measured spectrum. An "eyeball fit" in which

both the peak position (n) and spectrum width (E_0) were optimized give a 'best' fit with n=½ and E_0=2.5eV. The shape of the calculated Maxwellian distribution of secondary electrons does not agree well with the measurements in that it over predicts at low energies and under predicts at high energies. In the Hachenberg expression, the only adjustable parameter is the value of the work function of the target material (ϕ). The best "eyeball fit" agrees very well with the measured electron emission spectrum with a value for ϕ = 3.75eV. The work function of copper reported in the literature is ϕ_{Cu} = 4.0eV (unfortunately, the values reported in the literature vary considerably -- dependent on the condition of the copper sample examined). It is clear from the figure that the noise in the measurement data below 0.2 eV will limit the accuracy of the secondary emission coefficient (δ) calculated by integrating the measured emission energy distribution. In the copper example above, less than 1% of the secondary electron emission coefficient comes from electrons with energies less than 0.2eV.

Conclusion:

In all cases presented, the integrated secondary yield data falls between the values calculated using the Katz and Sternglass/Prokopenko expressions, while the shape of the low energy emission spectrum agrees well with the expression of Hachenberg. The question remains as to whether these measurements are relevant to secondary and backscatter emission yields from spacecraft metal surfaces. The production of the secondary and backscatter emission electron can be considered as a two step process: the creation of the secondary electron within the bulk material followed by the subsequent escape of the secondary electron from the bulk surface. The latter process is very dependent on the surface/vacuum interface. Davies and Dennison[5] demonstrated that the secondary electron production coefficient for aluminum decreased by over 40% from its clean value when contaminated by outgassing from a small piece of PTFE.

In LEO, the spacecraft surface is continually 'scrubbed' by atomic oxygen and UV photons and continually contaminated by spacecraft effluence (for the most part of unknown composition). How well the laboratory measurements of σ for a particular maaterial will predict the actual yield of the same material on orbit is unknown. Since spacecraft charging codes (NASCAP) have been very successful in predicting charging events, it is possible that the difference in yield between a 'clean' and a 'dirty' surface may only enter the spacecraft charging equation as a time scale factor, i.e., the absolute value of σ only affects the time scale over which the charging event will occur and not whether it will occur. Likewise, the movement of σ across the σ = 1 boundary (due to contamination) will change which part of the incident energy distribution will drive the charging event -- which can again be viewed as a time scale shift.

==========

1. Katz, I., Parks, D. E., Mandell, M. J., Harvey, J. M., Brownell Jr., D. H., Wang, S. S., and Rotenberg, M., A Three Dimensional Dynamic Study of Electrostatic Charging in Materials, NASA CR-135256, SSS-R-77-3367

2. Sternglass, E. J., "Backscattering of Kilovolt Electrons from Solids," Phys. Rev., Vol. 95, No. 2, p 345, July 1954.

3. Prokopenko, S. M. L. and Laframboise, J. G., "High-Voltage Differential Charging of Geostationary Spacecraft," Journal of Geophysical Research, Vol 85, No. A8, p 4125, Aug 1980.

4. Hachenberg, O. and Brauer, W., "Secondary Electron Emission form Solids," Advances in Electronics and Electron Physics, Vol.16, p 145, 1962.

5. R.E. Davies and J. R. Dennison, "Evolution of Secondary Electron Emission Characteristics of Spacecraft Surfaces", J. Spacecraft, Vol 34, No 4, 1997, p 571-574.